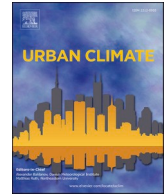




ELSEVIER

Contents lists available at [ScienceDirect](https://www.sciencedirect.com)

## Urban Climate

journal homepage: [www.elsevier.com/locate/uclim](http://www.elsevier.com/locate/uclim)

# Impacts of anthropogenic aerosols on orographic precipitation in Arizona

Juan J. Henao<sup>a,\*</sup>, John F. Mejia<sup>b</sup>, Frank McDonough<sup>b</sup>

<sup>a</sup> Escuela Ambiental, Facultad de Ingeniería, Universidad de Antioquia, Medellín, Colombia

<sup>b</sup> Division of Atmospheric Sciences, Desert Research Institute, Reno, NV, USA

## ARTICLE INFO

### Keywords:

Aerosol-cloud interactions  
WRF-Chem  
Spillover effect  
Orographic precipitation

## ABSTRACT

Water resources are limited in the fast-growing western United States, where increasing drought and warming temperatures are accelerating water losses. In addition, changes in the types and numbers of airborne aerosols can reduce the ability of clouds to efficiently produce precipitation. In this study, we use a cloud-resolving configuration of the Weather Research and Forecasting Model coupled with chemistry to analyze the impacts of anthropogenic aerosols from the urban area of Phoenix on orographic precipitation in the surrounding mountains. Two experiments including aerosol-radiation and aerosol-cloud interactions were performed, one with anthropogenic emissions and the other without anthropogenic emissions. The simulations are performed at 3 km resolution, from March 10–15, 2019. In addition, to assess these interactions for a longer period at a lower computational cost, we employed a four-month dispersion model based on Lagrangian trajectories.

The simulations show that aerosols emitted from the Phoenix urban area can reach the windward side of the Mogollon Rim (NE of Phoenix) and interact with supercooled liquid water environments. In this area, the simulation with full emissions results in less frozen precipitation on the windward side of the mountains (~9%) and a mild increase in frozen precipitation on the lee side (~8%), consistent with the “spillover” effect. The simulation with the Lagrangian model shows that aerosols emitted from Phoenix constantly reach the mountains near Phoenix, are distributed at heights up to 4-km and enter environments with supercooled liquid water, where aerosol-cloud-precipitation interactions can be strong. This study shows that air pollution from Phoenix can impact winter precipitation in the mountains downwind, affecting the spatial distribution of precipitation in an area with scarce water resources.

## 1. Introduction

Access to fresh clean water supplies is critical for life, health, and ecosystems. In the fast-growing western United States (US), water resources are especially limited and have been shown to be decreasing over the past several decades (Huning and AghaKouchak, 2020; Mote et al., 2018). In many parts of the West, water demand often outstrips allocations leading to significant economic and environmental losses. To maintain economic stability, healthy forests, fisheries, and the region’s diverse ecosystems, long-term consistent water supplies are critical.

\* Corresponding author.

E-mail address: [jose.henao@udea.edu.co](mailto:jose.henao@udea.edu.co) (J.J. Henao).

<https://doi.org/10.1016/j.uclim.2023.101561>

Received 9 February 2022; Received in revised form 19 September 2022; Accepted 16 May 2023

Available online 19 May 2023

2212-0955/© 2023 The Authors. Published by Elsevier B.V. This is an open access article under the CC BY-NC-ND license (<http://creativecommons.org/licenses/by-nc-nd/4.0/>).

A significant source of the scarce water supplies across the western US are from annual winter snowfall over the high mountains of the region (Bales et al., 2006). Historically, snowfall accumulates over the winter and spring. In recent years, periodic and increasing drought and warming temperatures are accelerating water losses, causing additional water stress (Harpoled et al., 2012). Climate changes studies suggest that the Southwest will be influenced by higher temperatures, decreased precipitation, and subsequent reduced water supplies (USGCRP, 2018). A compositing study using precipitation measurements concluded that air pollution from Phoenix suppressed local-area winter precipitation (Svoma and Balling, 2009). For Phoenix, intense water supply and water conservation strategies appear to be encouraging (City of Phoenix, 2021; Hornberger et al., 2015). It is possible, however, that less studied considerations of the urban air pollution in the surrounding hydrologic and ecologic systems are as significant as those expected by climate change, regional climate trends, and those related by the urban growth and its urban heat island effects (Chow et al., 2012).

Changes in the types and numbers of certain types of airborne aerosols (both man-made air pollution and increasing dust from winds blowing across dry and disturbed land) are reducing the ability of clouds to efficiently produce precipitation (Rosenfeld et al., 2008). Notwithstanding, the type of aerosols and environmental conditions can lead to contrasting results (Choudhury et al., 2019; Jha et al., 2021; Khain, 2009; Lohmann, 2017; López-Romero et al., 2021). In the case of winter snowfall over the western US, this air pollution is expected to further decrease the critical snowpack in the windward side of the mountains, according to observations and model simulations (Borys et al., 2000; Jha et al., 2021; Jirak and Cotton, 2006; Lynn et al., 2007; Rosenfeld and Givati, 2006; Saleeby et al., 2011, 2013; Svoma and Balling, 2009). This phenomenon has been referred to as “spillover” effect or the “riming indirect” effect (Lohmann, 2017; Saleeby et al., 2011), as it occurs due to reduced riming rates because of smaller droplets, which delays precipitation and cause a spillover to the lee side of the mountains (Lohmann, 2017). Lynn et al. (2007) performed numerical simulations to study the effects of air pollution on precipitation in the Sierra Nevada mountains, finding that aerosols reduce precipitation on the windward side and shift the maximum precipitation downwind, consistent with the spillover effect. This occurred in their simulations due to less efficient droplet freezing of smaller particles, producing less graupel but more ice and snow, which do not grow large enough to precipitate and are advected downwind. Similarly, the numerical simulations of Saleeby et al. (2013, 2011) in the Colorado mountain range show that high aerosol concentrations tend to impede the riming process, resulting in unrimed or lightly rimed ice hydrometeors with a lower density and slower sedimentation velocities. This results in reduced precipitation amounts on windward slopes, mainly of graupel, and enhanced precipitation amounts on leeward slopes, mainly of snow (Saleeby et al., 2013). This spillover effect was found to be higher in mountains with high cloud water paths and ice water paths (Saleeby et al., 2011). However, the numerical simulations of Fan et al. (2017, 2014) found increases in precipitation with increasing pollution over the Sierra Nevada Mountains, due to increases in snow formation caused by dust particles acting as ice nuclei. In their simulations, total precipitation increased by 10–20%. These results agree with observational studies supporting the idea that the presence of dust increases precipitation and snowpack (Ault et al., 2011; Creamean et al., 2013).

This study analyzes the effects of anthropogenic air pollution from Phoenix and nearby areas on orographic precipitation in the surrounding mountains, using a cloud-resolving configuration of the Weather Research and Forecasting Model coupled with chemistry, and a Lagrangian dispersion model. Here, we use the model to test the significance and regional extend of Svoma and Balling (2009) results by comparing precipitation changes in a simulation with full anthropogenic emissions and other without anthropogenic emissions. Modeling studies are relevant as estimating the effects of air pollution in precipitation from observations is a challenging task and there is significant controversy (e.g., Alpert et al., 2008; Khain, 2009). We use the model to examine the spillover effect in the mountainous areas downwind from Phoenix. Further, we employ a dispersion model to estimate the likelihood in which aerosols emitted from Phoenix can reach the surrounding mountains at elevations where they can influence mixed-phase orographic clouds.

## 2. Observations and methodology

### 2.1. WRF-Chem simulations

The numerical simulations are performed with the Weather Research and Forecasting Model coupled with chemistry (WRF-Chem; Grell et al., 2005) version 4.1.1. Aerosol and gas-phase chemistry are simulated with the Model for Simulating Aerosol Interactions and Chemistry (MOSAIC; Zaveri et al., 2008) aerosol model and with the Carbon-Bond Mechanism version Z (CBMZ; Zaveri and Peters, 1999) mechanism, respectively. CBMZ uses the lumped structure approach for condensing organic species and reactions, that includes 67 species and 164 chemical reactions in the augmented version coupled with MOSAIC (Zaveri et al., 2008). The selected MOSAIC configuration uses a sectional approach to represent aerosol size distributions in eight discrete size bins, with lower and upper bin limits based on dry particle diameters ( $D_p$ ; Zaveri et al., 2008). All particles within a bin are assumed to have the same chemical composition (internally mixed), while particles in different bins are externally mixed.  $D_p$  range from 39 nm to 10  $\mu\text{m}$ , with six bins for  $D_p < 2.5 \mu\text{m}$  and two bins for  $D_p$  larger than 2.5  $\mu\text{m}$ . MOSAIC includes all the major organic and inorganic aerosol species that are considered relevant at urban, regional, and global scales (Zaveri et al., 2008).

Aerosol-Radiation and Aerosol-Cloud interactions (ACI) are included following Fast et al. (2006) and Chapman et al. (2009). Aerosol radiation interactions are included by coupling simulated cloud droplet number with the RRTMG shortwave radiation scheme and the Lin microphysics scheme, with aerosol optical properties based on Mie theory (Fast et al., 2006). In this model configuration, aerosol particles act as cloud condensation nuclei (CCN) affecting cloud droplet number and radiative properties, while clouds can modify aerosol size and composition through aqueous reactions and wet scavenging (Chapman et al., 2009). Aerosol size distribution and composition contribute to the determination of CCN, and aerosols activation, when aerosol particles form cloud droplets, and aerosol resuspension, when the cloud dissipates in a grid-cell and aerosols are resuspended to the interstitial air, are associated with the vertical transport (Chapman et al., 2009). Aerosol activations and resuspension rates are calculated simultaneously with the turbulent

vertical mixing, and the interstitial and cloud-borne aerosols are determined at each time step and are size resolved. When WRF-Chem is configured to include ACI, the Lin microphysics scheme includes a two-moment treatment of cloud water (cloud water mass and cloud droplet number), which includes water vapor, cloud water, rain, cloud ice, snow and graupel. Dry and wet deposition processes for gas and aerosol species are included, as well as cloud chemistry processes. Photolysis rates are calculated with the Fast-J scheme (Wild et al., 2000). Predicted aerosol particles do not directly influence ice nuclei (IN), as it is not available in current versions of WRF-Chem, but ice clouds are included in the Lin scheme using the IN distribution prescribed in the scheme.

Anthropogenic aerosol and trace gas emissions come from the Emission Database for Global Atmospheric Research with Task Force on Hemispheric Transport of Air Pollution (EDGAR-HTAP; Janssens-Maenhout et al., 2015) for the base year 2010 (v2.2), scaled with monthly activity factors and with a horizontal spatial resolution of 0.1°. The speciation of non-methane volatile organic compounds emissions is done using the WRF\_UoM\_EMIT emission preprocessing tool ([https://github.com/douglowe/WRF\\_UoM\\_EMIT](https://github.com/douglowe/WRF_UoM_EMIT)), which is based on the EDGAR v4.3.2 inventory (Huang et al., 2017) and has been implemented in several studies (e.g., Chen et al., 2020; Jat et al., 2021). Biogenic emissions come from the Model of Emission of Gases and Aerosol (MEGAN) for biogenic emissions (Guenther et al., 2006), and fire emissions were not included as are not relevant for the study period.

Chemical initial and boundary conditions are obtained from the Community Atmosphere Model with chemistry (CAM-chem; Buchholz et al., 2019; Emmons et al., 2020), that has a horizontal spatial resolution of  $0.9 \times 1.25$ , 56 vertical levels, and a temporal resolution of 6 h. Meteorological initial and boundary conditions come from the North American Regional Reanalysis (NARR; Mesinger et al., 2006), produced and recurrently updated by the National Centers for Environmental Prediction. NARR has a horizontal spatial resolution of 32 km and 45 vertical layers. NARR provides lateral boundary conditions of surface, atmospheric, and soil variables for

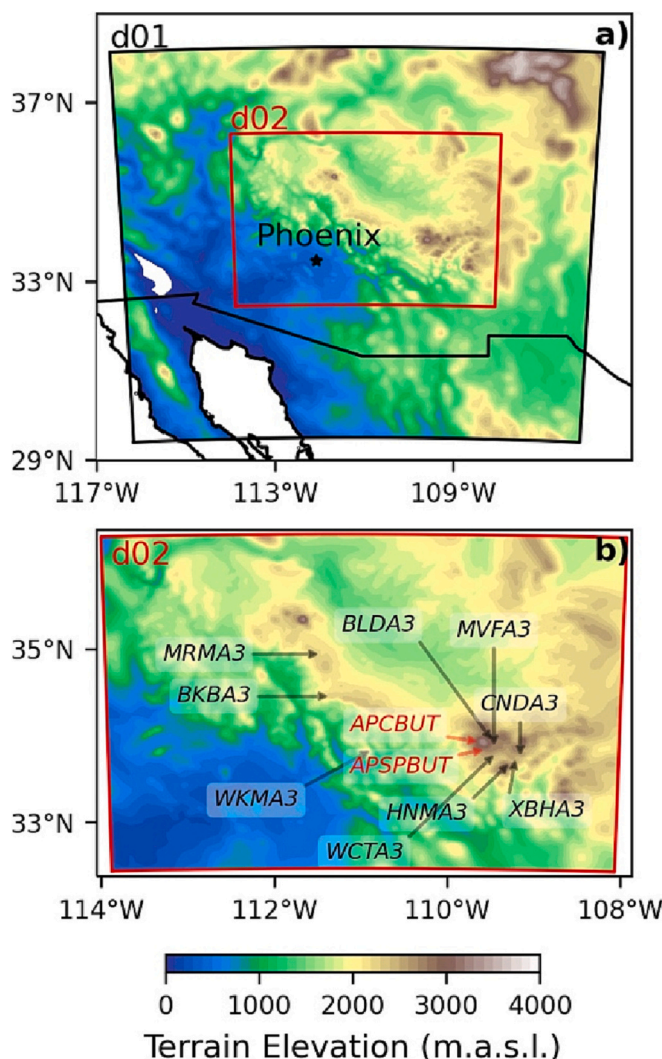


**Fig. 1.** (a) Simulation domains with horizontal resolutions of 9 km (d01) and 3 km (d02). Colour shades show terrain elevation. (b) Location of the available SNOTEL (black) and SRP (red) stations in domain d02. (For interpretation of the references to colour in this figure legend, the reader is referred to the web version of this article.)

domain 1, updated every three hours.

The model domains are shown in Fig. 1. Two one-way nested domains are included, with horizontal grid resolutions (grid points) of 9 km (110 × 110) and 3 km (184 × 145), respectively, and 65 vertical levels with the model top at 50 hPa. The parameterizations used are listed in Table 1.

Two experiments were developed to study the effects of anthropogenic aerosols from Phoenix and the surrounding urban areas on the precipitation forming downwind. One simulation includes full emissions and boundary conditions, hereafter referred to as *Anthro*; a second simulation is performed with neither anthropogenic emissions nor boundary conditions, hereafter referred to as *No Anthro*. Simulations are run for a 5-day period, from March 10 (00 UTC) to 15 (00 UTC) 2019, when various precipitation events occurred.

### 2.2. Observations

The model performance evaluation is done using the Snowpack Telemetry (SNOTEL) network operated by the Natural Resources Conservation Service. Eight SNOTEL sites from the available stations in the simulation domain d02 were considered for comparisons with modeled precipitation (Fig. 1b), while four stations were removed from the analysis due to no-data voids (> 25%) or data quality issues. Two additional stations from the Salt River Project (SRP, <https://srpnet.com>) are included in the analysis, both equipped with NOAA II All-Weather Precipitation Gauges (ETI instruments). Further details of the used stations are presented in Table 2. We did not include raingauges from other observation networks as the focus of the study is the spillover effect, which is related to frozen precipitation.

For the model evaluation we used the mean bias error (MBE), the root-mean-square error (RMSE) and the Pearson correlation coefficient (Cor), calculated as follows

$$MBE = \frac{1}{N} \sum_{i=1}^N (F_i - O_i) \tag{1}$$

$$RMSE = \sqrt{\frac{1}{N} \sum_{i=1}^N (F_i - O_i)^2} \tag{2}$$

$$Cor = \frac{\sum_{i=1}^N (O_i - \bar{O})(F_i - \bar{F})}{\sqrt{\sum_{i=1}^N (O_i - \bar{O})^2} \sqrt{\sum_{i=1}^N (F_i - \bar{F})^2}} \tag{3}$$

using N number of prediction-observation (F – O) pairs.

### 2.3. Analysis of precipitation changes

For the analysis of changes of precipitation and the spillover effect, we considered two different areas where the analyses are performed. One of these areas is chosen to include Phoenix and the areas downwind at higher elevations, where aerosols from the urban area can be directly transported and affect orographic precipitation (red box in Fig. 2a). The orientation of this area is selected to be approximately parallel to the mean wind flow. Further, to evaluate changes in windward and leeward areas, we classified model grid cells by their aspects using terrain elevation gradients. The aspect for each grid cell is defined by the maximum elevation difference with the eight-surrounding grid cells and limited to slopes larger than 1%. Based on the mean wind flow, windward grid cells have aspects classified as W, SW or S, while leeward grid cells have aspects classified as E, NE or N (Fig. 2b). The analysis in leeward and windward grid cells is focused on an area with significant precipitation and located at higher elevations downwind of Phoenix (dotted line in Fig. 2a). Results were invariant upon repeating this procedure after smoothing out the terrain aspects.

**Table 1**  
Selected model configuration options for the WRF-Chem simulations.

Process	WRF-Chem option (Reference)
Microphysics	Extended Lin (Chapman et al., 2009; Chen and Sun, 2002)
Longwave Radiation	RRTMG (Iacono et al., 2008)
Shortwave Radiation	RRTMG (Iacono et al., 2008)
Surface Layer	Monin-Obukhov Janjic Eta (Janjić, 1994)
Land Surface	Noah-MP (Niu et al., 2011)
Boundary layer (PBL)	MYJ (Janjić, 1994)
Cumulus (d01 only)	New Grell (Grell and Dévényi, 2002)

**Table 2**  
List of included precipitation sites.

Station ID	Type	Station name	Latitude	Longitude	Elevation [m]
BKBA3	SNOTEL	Baker Butte	34.45547	-111.40643	2225
BLDA3	SNOTEL	Baldy	33.97883	-109.50344	2781
MRMA3	SNOTEL	Mormon Mountain	34.94109	-111.51849	2286
WKMA3	SNOTEL	Workman Creek	33.81242	-110.91773	2103
MVFA3	SNOTEL	Maverick Fork	33.92121	-109.45881	2804
CNDA3	SNOTEL	Coronado Trail	33.80392	-109.15282	2560
XBHA3	SNOTEL	Beaver Head	33.69144	-109.21657	2435
HNMA3	SNOTEL	Hannagan Meadows	33.65387	-109.30952	2749
WCTA3	SNOTEL	Wildcat	33.75835	-109.47973	2392
ASPBUT	SRP	Aspen Butte	33.82903	-109.61008	2625
APCBUT	SRP	Apache Butte	33.93853	-109.67679	2896

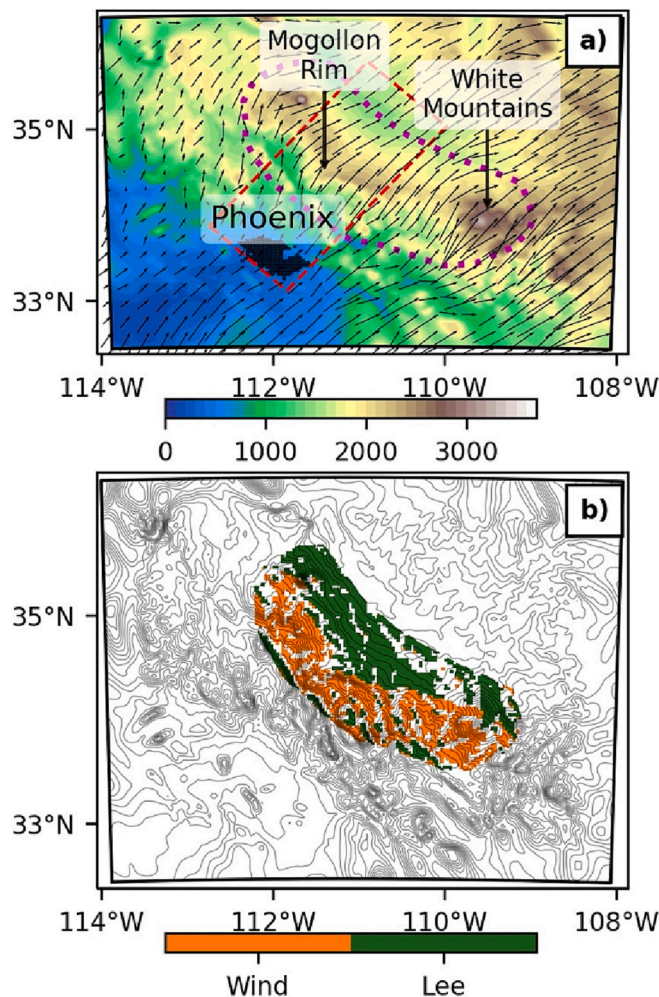


**Fig. 2.** (a) Mean near surface wind vectors (first 4 model levels) in domain d02, and areas of interest named in the text. The red box and the dotted line show the areas of interest where further analyses are focused. (b) Aspect orientation (windward or leeward) of grid cells with slopes larger than 1%. (For interpretation of the references to colour in this figure legend, the reader is referred to the web version of this article.)

#### 2.4. WRF-standard simulation and dispersion model

To assess how aerosols emitted from Phoenix interact with mixed-phase clouds and precipitating systems in the study region for a longer period than the WRF-Chem simulations (section 2.1), but at a lower computational cost, we employed a dispersion model based on Lagrangian trajectories (described below) driven with meteorology from a simulation with the standard WRF model (hereafter

WRF-Standard). The Lagrangian dispersion model was forced with cloud-resolving WRF-Standard simulations integrated for the 2018 winter season, between December 1, 2018 and March 31, 2019. The WRF-Standard model configuration has same resolution, domains and meteorological initial and boundary conditions of the WRF-Chem configuration, but it has some differences in the selection of the physical parameterizations. These differences occur due to the limitations of the WRF-Chem model configuration, especially when aerosol-cloud interactions are included as it only works for selected parameterizations. For the WRF-Standard, all physics options are available and the selection of the schemes was based on previous experience for the region. The processes that were represented with different schemes in the WRF-Standard simulation are presented in Table 3.

Trajectories were tracked using a Lagrangian Stochastic Particle Tracking model (Henao et al., 2020; Mejia et al., 2019) that was integrated continuously using WRF-Standard 3-D model output at hourly time increments. Aerosols were released from the Phoenix urban areas at a rate proportional to the CO emissions as prepared for the WRF-Chem Anthro simulation. This Lagrangian model system considers turbulence diffusion and neglects deposition of particles. Particles were tracked until they reached a simulated cloud, with the locations and environments of particles colliding with clouds recorded. A volume kernel estimating particle number concentrations was then applied to all particles. This approach allows us to estimate number concentrations of particles reaching supercooled liquid water environments and how they relate to orographic cloud environments.

### 3. Results

#### 3.1. WRF-Chem simulations with aerosol-cloud interactions

Fig. 3 presents the time series of accumulated model precipitation along with measurements at different sites, and Table 4 presents the resulting error metrics for the Anthro and No Anthro simulations. The simulation period has a substantial amount of precipitation at these sites, with accumulations ranging from 53 to 127 mm, mainly falling between March 11 and 14. The model adequately simulated the timing and intensities of the precipitating system at BKBA3 and MRMA3, both sites relatively close to Phoenix (inside the red box area) and located at relatively lower elevations (~2200 m; Table 2). The model resulted in an earlier onset of precipitation at the highest sites, BLDA3, MVFA3, ASPBUT and APCBUT in the White Mountains, leading to overestimations despite similar total accumulated precipitation at the Baldy site (BLDA3). East of Phoenix, at WKMA3, there is also an earlier onset that leads to overestimations, but the timing of the most intense episodes coincides (slopes agree well). Sites to the southeast of the White Mountains (HNMA3 and XBHA3) evidence larger model overestimations, although there is an adequate representation (accumulated and timing) at CNDA3. Despite the relatively large overestimations at several sites, the model shows a reasonable performance of the precipitating systems over the study region, especially downwind from Phoenix in the area of interest.

Total accumulated precipitation from the Anthro and No Anthro simulations is shown in Fig. 4. In broad perspective, both simulations agree on the spatial distributions and accumulations of precipitation, which is mostly falling in areas located at higher elevations. There are significant amounts falling on the windward side of the Mogollon Rim, but the largest accumulations occur to the southeast of the domain, around the White Mountains, where in both simulations there are areas with over 250 mm of accumulated precipitation.

The number concentration of activated aerosol particles (aerosol in cloud) and total aerosol number concentration are shown in Fig. 5. Most aerosol particles in clouds are located to the south of the domain, around the domain southern limits, but also with large values around Phoenix (lower part of the red box), and in the windward side of the Mogollon Rim (downwind from Phoenix) where terrain elevations range between 1500 and 2000 m (Fig. 5a). Total aerosol number concentrations are concentrated around Phoenix (Fig. 5b), around the area with the highest emissions, but there are also large concentrations to the north of the area of interest, but with much fewer aerosol particles being activated in clouds. In general, for the areas of interest, activated aerosol particles are found to the south of the Mogollon Rim and the surrounding mountains, i.e., at the windward side of the slopes.

The differences in the resulting precipitation between the Anthro and No Anthro simulations are shown in Fig. 6. The contrasting aerosol loadings of both simulations lead to increases and decreases of rainfall and frozen precipitation (Anthro - No Anthro), depending on the region. The domain-averaged change in total precipitation is  $-0.4$  mm, but there are differences of over  $\pm 40$  mm in total accumulated precipitation at some locations. Around Phoenix, where aerosol loadings are higher, there is a decrease in precipitation (rainfall in this area) of around 5 mm (Fig. 6a), although this area received relatively little precipitation on both simulations. Around this area (lower part of the red box in Fig. 6a), rainfall is mostly reduced, but there are also parts of this area where rainfall increased. To support this idea, Fig. 7 shows the differences in rainfall for model grid cells with urban land covers and other land covers around Phoenix. The urban area is characterized by decreases in rainfall, with only a few grid cells showing increases. For other land covers, there is still a general decrease, but there is a larger portion of grid cells showing increases in rainfall and a larger variability.

In contrast to rainfall, for frozen precipitation there is a clear pattern in the differences in the areas of interest (Fig. 6b), where the windward side of the slopes show decreases, while leeward areas show increases. Especially in the central part of the red box, there are

**Table 3**  
Selected model configuration options for the WRF-Standard simulation.

Process	WRF-Standard option (Reference)
Microphysics	Thompson (Thompson et al., 2008)
Longwave Radiation	RRTM (Mlawer et al., 1997)
Shortwave Radiation	Dudhia buscar (Dudhia, 1989)

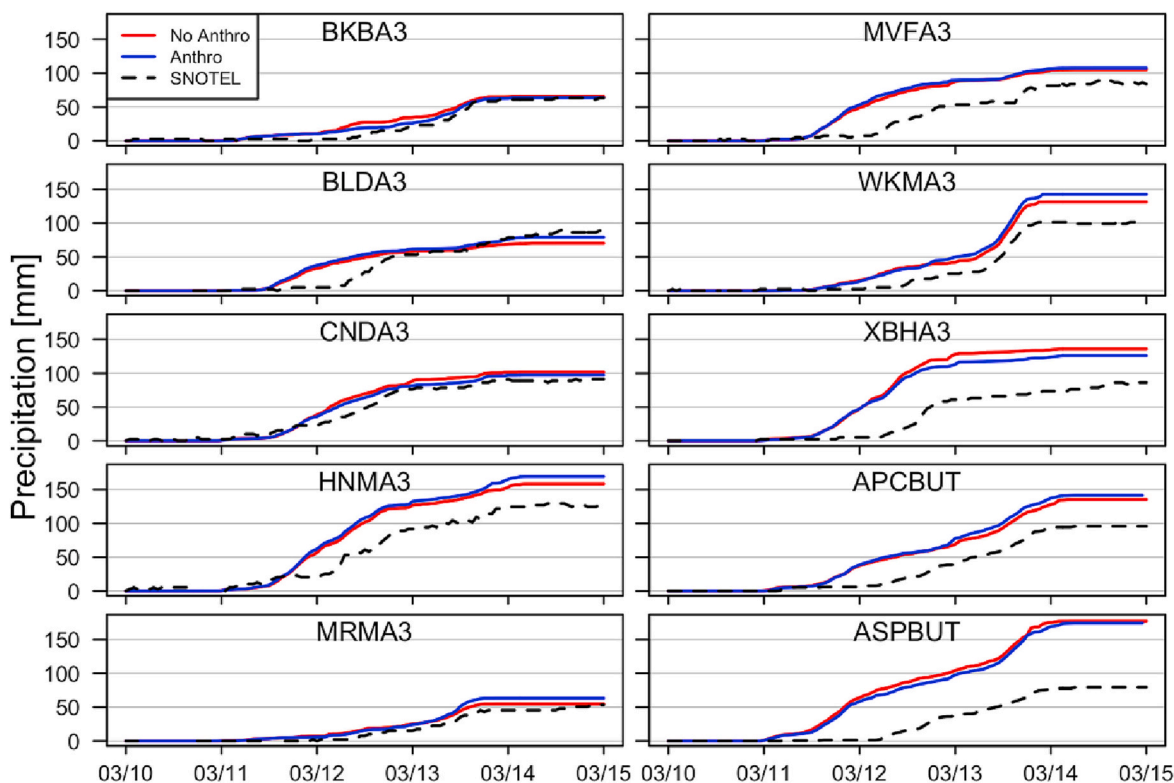


Fig. 3. Time series (March 2019) of accumulated precipitation in the included sites indicated in Fig. 1 and the Anthro and No Anthro simulations. Model precipitation corresponds to the closest grid cell. Site identifiers (as in Table 2) are annotated at the top of each panel.

Table 4  
Error metrics of observed and WRF-Chem modeled total precipitation (P in mm).

Station	Type	RMSE - Anthro	BIAS - Anthro	Cor - Anthro	RMSE - NoAnthro	BIAS - NoAnthro	Cor - NoAnthro
BKBA3	SNOTEL	5,67	3,60	0,99	8,75	5,89	0,97
BLDA3	SNOTEL	14,86	6,70	0,92	14,48	2,74	0,92
CNDA3	SNOTEL	8,15	4,62	0,99	11,84	7,78	0,99
HNMA3	SNOTEL	34,36	26,89	0,98	28,49	21,87	0,98
MRMA3	SNOTEL	11,04	9,02	0,99	7,19	6,26	0,99
MVFA3	SNOTEL	28,52	22,33	0,93	26,10	20,38	0,94
WKMA3	SNOTEL	26,03	19,57	0,99	20,32	15,68	0,99
XBHA3	SNOTEL	45,54	39,69	0,93	53,38	46,53	0,93
ASPBUT	SRP	61,32	49,67	0,96	66,14	54,17	0,96
APCBUT	SRP	31,77	25,55	0,98	27,79	22,61	0,98
<b>Average</b>		<b>26,73</b>	<b>20,76</b>	<b>0,97</b>	<b>26,45</b>	<b>20,39</b>	<b>0,96</b>

reductions in frozen precipitation to the SW of the dotted line (2000 m contour) and increases to the NE. This spatial pattern is consistent with the concept of the spillover effect. The differences between simulations for snow water equivalent are consistent with those of frozen precipitation (not shown).

To better understand the differences at windward and leeward areas for the area of interest, the distributions of precipitation differences are shown in Fig. 8, classified into leeward and windward using the aspect of each grid cell. Most windward grid cells present decreases in frozen precipitation, having a negative median and resulting in a mean decrease of 8.8%, while most leeward grid cells show little change, but with a positive median and a mean increase of 7.8%. Rainfall distributions are similar for windward and leeward grid cells, although there are more windward grid cells showing increases. This result is related to the high spatial variability in rainfall changes seen in Fig. 6a, where the only clear pattern is the decrease in Phoenix collocated with the highest emissions. For total precipitation, the effect is consistent with the spillover effect reported for frozen precipitation, having decreases for windward areas (−1.8%) and increases for the leeward areas (1%).

Fig. 9 shows the profiles of mixing ratio for snow and graupel in both simulations and their differences. In the No Anthro simulation, windward grid cells exhibit larger values for snow and graupel. Consequently, the increase in aerosol loadings lead to a decrease in graupel and snow in the windward areas, especially near the surface (< 1 km). For snow, windward grid cells show increases at higher

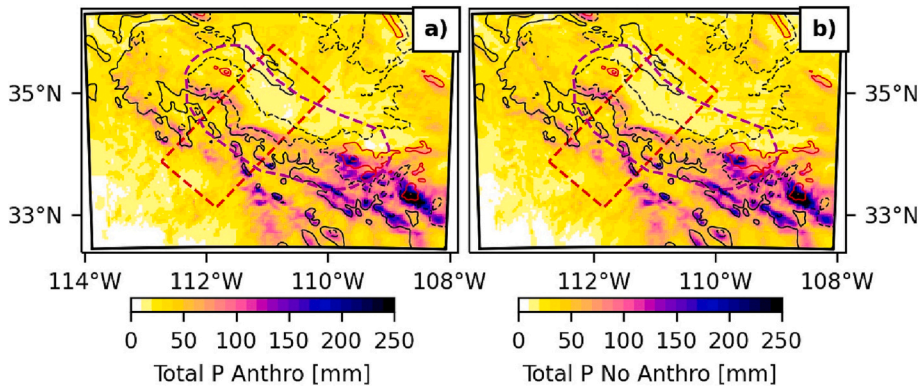


**Fig. 4.** Total accumulated precipitation (P) in the (a) *No Anthro* and (b) *Anthro* simulations. Contour lines show terrain elevation for levels of 1500 m (solid black), 2000 m (dotted black), 2500 m (solid red) and 3000 m (dotted red). (For interpretation of the references to colour in this figure legend, the reader is referred to the web version of this article.)

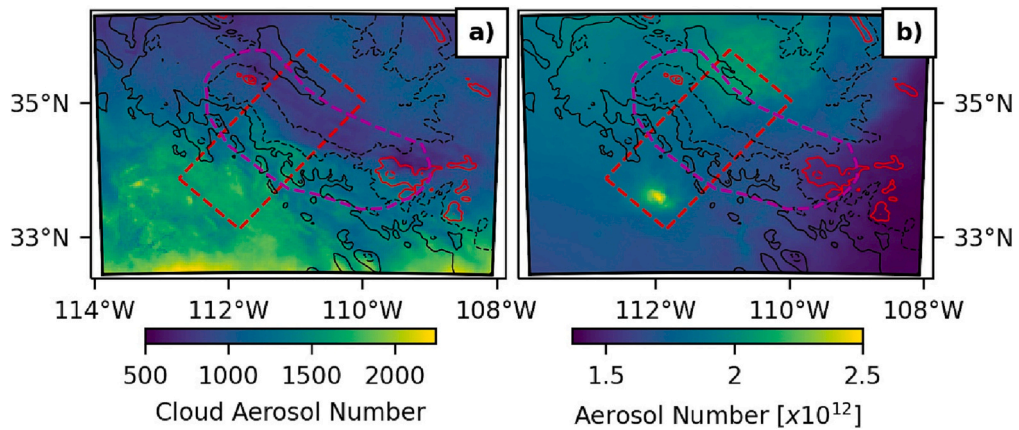


**Fig. 5.** Mean vertically integrated number concentrations of (a) aerosols in cloud and (b) total aerosol. Values considering all aerosol particle sizes. Contour lines show terrain elevation as in Fig. 4.

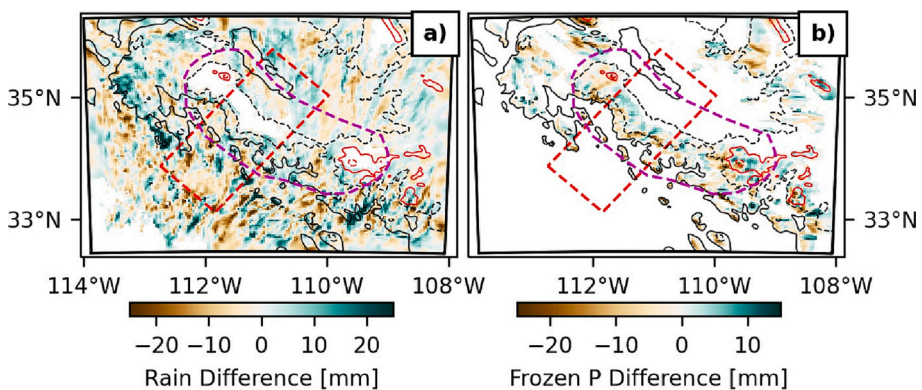


**Fig. 6.** Differences in (a) accumulated rainfall and (b) frozen precipitation (P) between the *Anthro* and *No Anthro* simulations. Differences are calculated over grid cells with  $P > 10$  mm in both simulations. Contour lines show terrain elevation as in Fig. 4.

elevations (around 5 km) and increases at leeward areas for elevations lower than 6 km. These results are consistent with the mechanisms of the spillover effect, in which aerosols reduce the rimming efficiency on windward areas, leading to decreases in graupel but increases in snow at higher elevations that can be advected further away to the lee side.

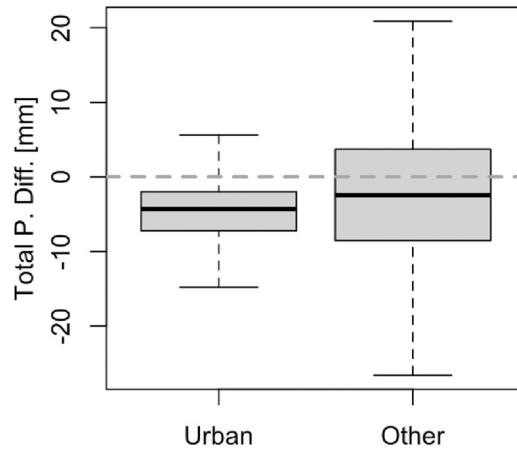


**Fig. 7.** Differences in precipitation between the Anthro and No Anthro simulations for urban and other grid cells around Phoenix. Values for a region of 40 km (radius) around Phoenix.

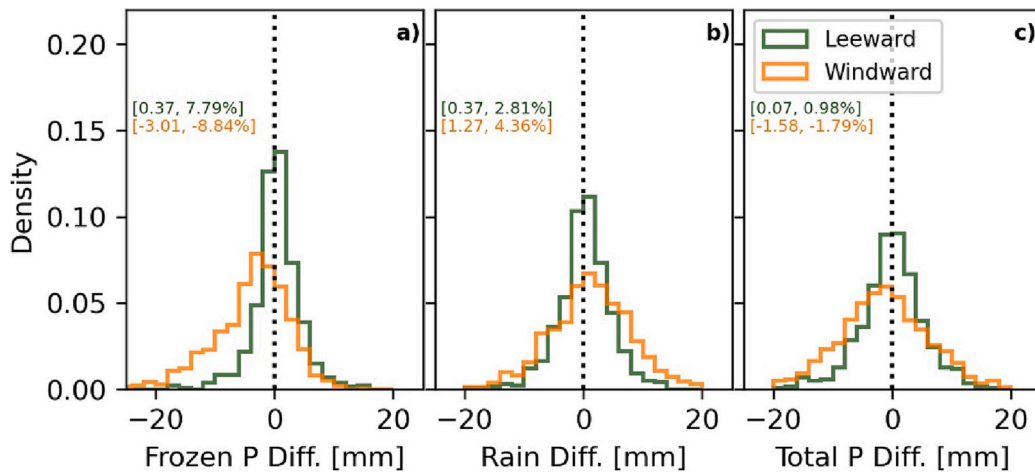


**Fig. 8.** Histograms of differences (*Anthro* minus *No Anthro*) in leeward and windward grid cells for (a) frozen precipitation (P), (b) rainfall, (c) and total accumulated P. Values in brackets indicate the median in mm and the mean percent difference, respectively.

### 3.2. Dispersion simulations

This section presents the results of the four-month dispersion simulation (Section 2.4) driven with meteorology from the WRF-Standard simulation. A comprehensive model evaluation using the available precipitation observations was performed to gain confidence in basic aspects of the WRF-Standard simulation for seasonal and day-to-day variability (Table 5). The WRF-Standard simulation results in better error metrics than the WRF-Chem simulation (except the correlation), and with less variation between sites, but still showing an overestimation at all sites. Having the same boundary conditions, the most probable explanation lies in the use of the Thompson microphysics scheme here, instead of the Lin that was used in WRF-Chem.

Fig. 10 shows the particle number concentration and the interceptions of emitted particles from Phoenix with supercooled liquid water environments. In general, particles from emitted Phoenix are dispersed long distances and can reach the lee side of the Mogollon Rim, but concentrations decrease rapidly by two-to-three orders of magnitude (Fig. 10a). It is noteworthy that particles emitted from Phoenix can be dispersed vertically up to 4 km in the mountains downwind, and are entrained into the orographic clouds, where they intercept supercooled liquid water layers (Fig. 10b). This interception tends to develop downwind from Phoenix at depths of 2–3 km, in the windward side of the southern slopes of the Mogollon Rim (Fig. 10b).

The flow characteristics and areas where aerosols interact with mixed-phase clouds shown in the relatively short WRF-Chem simulations do not only occur for that specific period and precipitating system, but are frequent for the precipitating events occurring during the winter season. Fig. 11 shows the total number of particle interceptions with supercooled liquid water environments for each month of the simulation, both for the entire domain and for the area of interest. The interceptions between particles from Phoenix and supercooled cloud layers (Fig. 10a) occur during the four months of the simulation (Fig. 11). Most interactions between particles and mixed-phase clouds occur between January and March, having similar monthly values for the entire domain, but with a clear peak

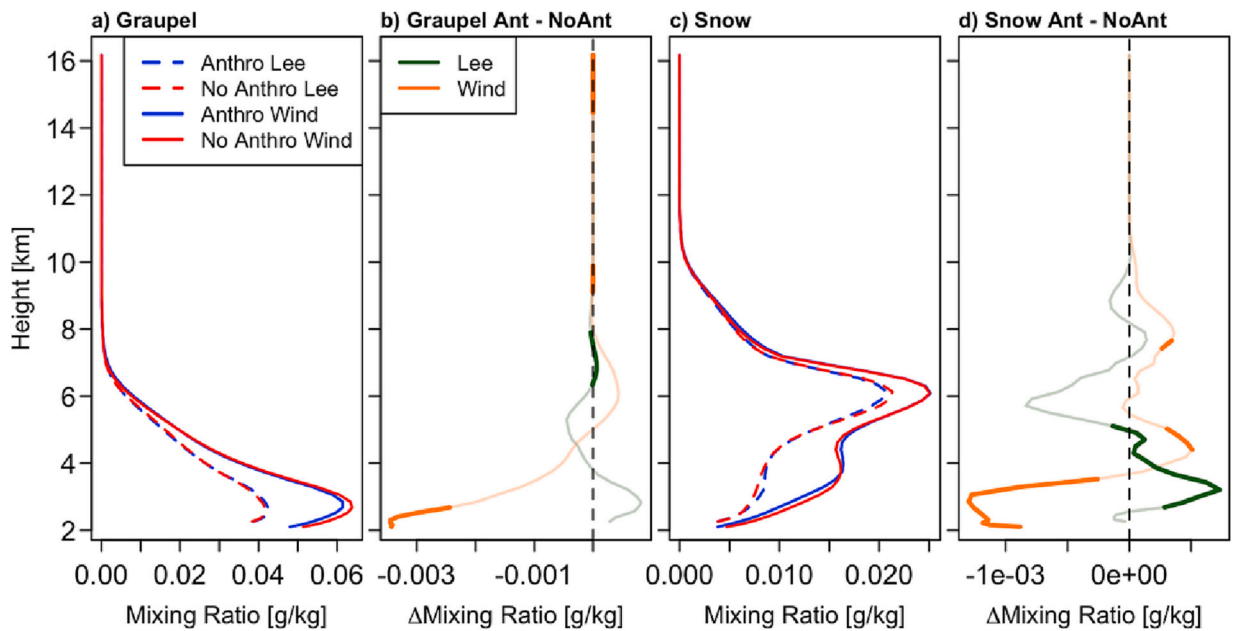


Fig. 9. Mixing ratio vertical profiles of (a) graupel, (b) graupel differences (Anthro minus No Anthro), (c) snow and (d) snow differences. Values composited by leeward and windward grid cells. Statistically significant differences in (b) and (d) are shown in thick lines.

Table 5

Observed and WRF-Standard modeled total precipitation (P in mm).

Station	Type	Total P Obs	Total P Mod	RMSE	BIAS	Cor
APCBUT	SRP	485	525	7,34	0,37	0,75
ASPBUT	SRP	423	473	7,02	0,46	0,72
BKBA3	SNOTEL	480	489	7,33	0,08	0,80
BLDA3	SNOTEL	358	397	6,04	0,37	0,71
CNDA3	SNOTEL	218	389	5,31	1,59	0,82
HNMA3	SNOTEL	422	489	6,62	0,63	0,81
MRMA3	SNOTEL	495	507	7,05	0,11	0,75
MVFA3	SNOTEL	361	452	6,72	0,86	0,71
WCTA3	SNOTEL	328	374	7,16	0,44	0,53
WKMA3	SNOTEL	490	530	7,54	0,37	0,82
XBHA3	SNOTEL	287	418	7,66	1,23	0,64
Average		395	459	6,89	0,59	0,73

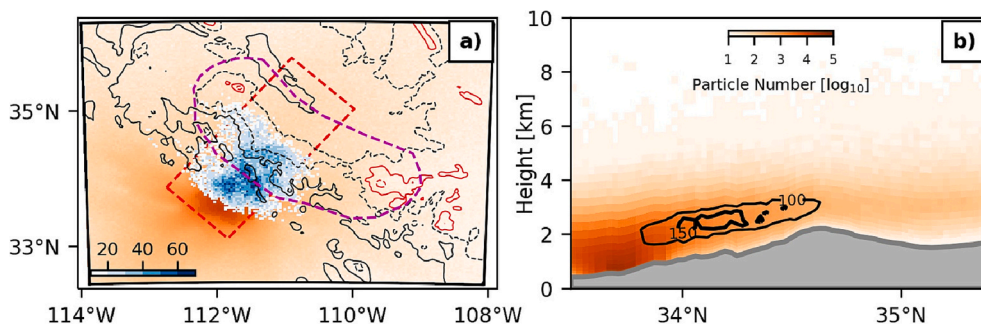
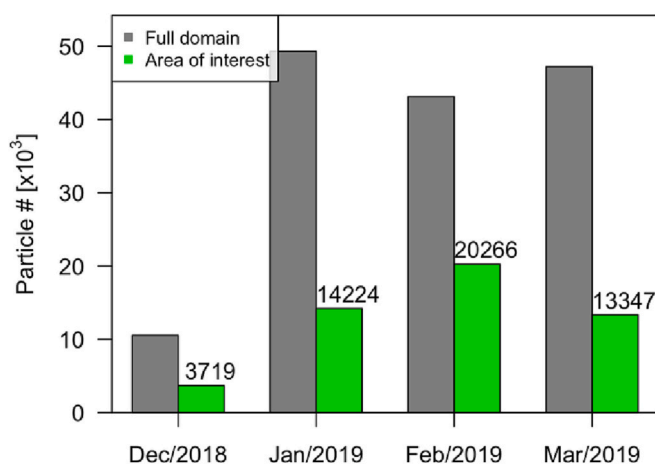


Fig. 10. (a) Horizontal vertically integrated total particle number concentration (orange contours) and total number of interceptions with supercooled liquid water environments (blue contours). (b) Same as in (a) but for an average transect downwind from Phoenix (red box in panel a). Black contours in (b) show the number of particle interceptions with supercooled liquid water environments. Note the logarithmic scale for particle number concentration in both panels. (For interpretation of the references to colour in this figure legend, the reader is referred to the web version of this article.)



**Fig. 11.** Total number of particle interceptions with supercooled liquid water environments per month of simulation. Area of interest refers to the mountainous region shown with the dotted line in Fig. 10a.

in February for the interactions occurring in the mountains around the area of interest.

#### 4. Conclusions and discussion

In this study, the WRF-Chem model was used to analyze the impacts of anthropogenic aerosols from the urban area of Phoenix on orographic precipitation in the surrounding mountains. Two experiments were performed, one with full anthropogenic emissions (Anthro) and the other without anthropogenic emissions (No Anthro), which were integrated between during a cold season storm event March 10 and 15, 2019. The model was configured to include aerosol-radiation and aerosol-cloud interactions, in which aerosol particles can act as cloud condensation nuclei, affecting cloud droplet numbers and radiative processes. WRF-Chem modeled precipitation agreed reasonably well with observations from the SNOTEL network, especially in the mountains downwind from Phoenix, but relatively large overestimations occurred to the southeast of the domain. Uncertainties in simulated precipitation in numerical models is related to various factors and it is difficult to be examined. These factors include scale issues, especially in complex terrain by comparing a point (gage) observation with the model pixel, moisture input from boundary conditions and deficiencies in the physical parameterizations. It is worth noting that the seasonal WRF-Standard simulation, which uses the Thompson microphysics scheme, resulted in a better performance as compared to the WRF-Chem simulations with the Lin scheme, highlighting the sensitivity of model precipitation to the selection of the microphysics scheme. It is common for numerical models to overpredict precipitation in steep terrain, and the results are within the range of values reported in numerical models (Sun and Liang, 2020; Toride et al., 2019).

It is found that anthropogenic emissions from Phoenix are transported downwind and reach the Mogollon Rim, to the northeast of Phoenix, where aerosols interact with orographic clouds. In these areas, the increased aerosol loadings of the Anthro simulation led to decreases of ~9% in frozen precipitation on the windward slopes, and to increases of about 8% on the leeside of the mountains, a phenomenon that has been referred to as the spillover effect. These changes in frozen precipitation are associated with reductions in the mixing ratios of frozen hydrometeors close to the surface in the windward side of the slopes, especially of graupel, but increases in snow at higher elevations, that can be transported further downwind to the leeside. These findings agree with previous modeling studies in western US, where the spillover effect was reported (Lynn et al., 2007; Saleeby et al., 2011, 2013). In addition, we found that anthropogenic emissions are associated with decreases in rainfall in the urban area of Phoenix, which agrees with the observational analysis of Svoma and Balling (2009).

The four-month meteorology simulation and a dispersion Lagrangian model system showed that particles emitted from the Phoenix urban area constantly reach the surrounding mountains, especially the southern slopes of the Mogollon Rim. In this region, orographic forcing is strong and particles reach cloud layers with supercooled liquid water, which are considered environments of relatively strong aerosol-cloud-precipitation interactions (Rosenfeld et al., 2007). The idea of this WRF-Standard simulation is not to compare it with the WRF-Chem simulation, which use slightly different configurations, but to show that these interactions with supercooled layers are frequent, and occur mostly between January and March.

This study shows that air pollution from Phoenix can influence the amounts and distribution of winter season orographic precipitation falling in the downwind mountains, which accumulates as snow and is an important source in an area with limited water availability. Water resources management in the region should not only consider the effects of a warmer climate but also the effects of air pollution in its hydroclimate. It is worth noting that this study did not consider the effects of predicted aerosol particles on ice nuclei (not available in WRF-Chem) and dust emissions acting as ice nuclei. Different results could be obtained under conditions with significant dust aerosols concentrations, as dust particles acting as ice nuclei could increase orographic precipitation (Creamean et al., 2013; Fan et al., 2014; Jha et al., 2021). Better representations of these processes and longer simulations are needed to provide further insights and more robust results to better understand the effects of aerosols on orographic precipitation. The model results of the

present study can be useful for designing observational studies or to complement the current networks to be able to identify changes in the spatial patterns in precipitation that are challenging with the available stations and due to the uncertainty associated with observational studies (e.g., Alpert et al., 2008; Khain, 2009; Svoma and Balling, 2009).

### CRedit authorship contribution statement

**Juan J. Henao:** Methodology, Software, Validation, Formal analysis, Data curation, Writing – original draft. **John F. Mejia:** Conceptualization, Software, Supervision, Resources, Funding acquisition, Writing – review & editing. **Frank McDonough:** Funding acquisition, Writing – review & editing, Conceptualization, Resources.

### Declaration of Competing Interest

The authors declare that they have no known competing financial interests or personal relationships that could have appeared to influence the work reported in this paper.

### Data availability

Data will be made available on request.

### Acknowledgements

This research was partially funded by the Department of Atmospheric Sciences of the Desert Research Institute. Juan J. Henao was partially funded by John Mejia discretionary funds and the Ministry of Science, Technology and Innovation of Colombia -MIN-CIENCIAS-. The SNOTEL data was obtained from the Synoptic's Mesonet API (<https://synopticsdata.com/mesonet-api>) and the Salt River Project (SRP, <https://srpnet.com>) provided the data from the APCBUT and ASPBUT stations.

### References

- Alpert, P., Halfon, N., Levin, Z., 2008. Does air pollution really suppress precipitation in Israel? *J. Appl. Meteorol. Climatol.* 47 (4), 933–943. <https://doi.org/10.1175/2007JAMC1803.1>.
- Ault, A.P., Williams, C.R., White, A.B., Neiman, P.J., Creamean, J.M., Gaston, C.J., Ralph, F.M., Prather, K.A., 2011. Detection of Asian dust in California orographic precipitation. *J. Geophys. Res.-Atmos.* 116 <https://doi.org/10.1029/2010JD015351>.
- Bales, R.C., Molotch, N.P., Painter, T.H., Dettinger, M.D., Rice, R., Dozier, J., 2006. Mountain hydrology of the western United States. *Water Resour. Res.* 42 <https://doi.org/10.1029/2005WR004387>.
- Borys, R.D., Lowenthal, D.H., Mitchell, D.L., 2000. The relationships among cloud microphysics, chemistry, and precipitation rate in cold mountain clouds. *Atmos. Environ.* 34, 2593–2602. [https://doi.org/10.1016/S1352-2310\(99\)00492-6](https://doi.org/10.1016/S1352-2310(99)00492-6).
- Buchholz, R., Emmons, L.K., Tilmes, S., The CESM2 Development Team, 2019. CESM2.1/CAM-chem Instantaneous Output for Boundary Conditions [WWW Document]. UCAR/NCAR - Atmospheric Chemistry Observations and Modeling Laboratory. Lat: 25 to 40, Lon: -120 to -100, March 2019. <https://doi.org/10.5065/NMP7-EP60> (accessed 12.15.20).
- Chapman, E.G., Gustafson, W.I.J., Easter, R.C., Barnard, J.C., Ghan, S.J., Pekour, M.S., Fast, J.D., 2009. Coupling aerosol-cloud-radiative processes in the WRF-Chem model: investigating the radiative impact of elevated point sources. *Atmos. Chem. Phys.* 9, 945–964. <https://doi.org/10.5194/acp-9-945-2009>.
- Chen, S.-H., Sun, W.-Y., 2002. A One-dimensional Time Dependent Cloud Model. *J. Meteorol. Soc. Japan. Ser. II* 80, 99–118. <https://doi.org/10.2151/jmsj.80.99>.
- Chen, Y., Wild, O., Ryan, E., Sahu, S.K., Lowe, D., Archer-Nicholls, S., Wang, Y., McFiggans, G., Ansari, T., Singh, V., Sokhi, R.S., Archibald, A., Beig, G., 2020. Mitigation of PM<sub>2.5</sub> and ozone pollution in Delhi: a sensitivity study during the pre-monsoon period. *Atmos. Chem. Phys.* 20, 499–514. <https://doi.org/10.5194/acp-20-499-2020>.
- Choudhury, G., Tyagi, B., Singh, J., Sarangi, C., Tripathi, S.N., 2019. Aerosol-orography-precipitation – a critical assessment. *Atmos. Environ.* 214, 116831 <https://doi.org/10.1016/j.atmosenv.2019>.
- Chow, W.T.L., Brennan, D., Brazel, A.J., 2012. Urban Heat Island research in Phoenix, Arizona: theoretical contributions and policy applications. *Bull. Am. Meteorol. Soc.* 93 (4), 517–530. <https://doi.org/10.1175/BAMS-D-11-00011.1>.
- City of Phoenix, 2021. City of Phoenix Water Resource Plan. <https://www.phoenix.gov/waterservice/2021%20City%20of%20Phoenix%20Water%20Resource%20Plan.pdf>.
- Creamean, J.M., Suski, K.J., Rosenfeld, D., Cazorla, A., DeMott, P.J., Sullivan, R.C., White, A.B., Ralph, F.M., Minnis, P., Comstock, J.M., Tomlinson, J.M., Prather, K.A., 2013. Dust and biological aerosols from the Sahara and Asia influence precipitation in the Western U.S. *Science* 339, 1572–1578. <https://doi.org/10.1126/science.1227279>.
- Dudhia, J., 1989. Numerical study of convection observed during the winter monsoon experiment using a mesoscale two-dimensional model. *J. Atmos. Sci.* 46 (20), 3077–3107. [https://doi.org/10.1175/1520-0469\(1989\)046<3077:NSOCOD>2.0.CO;2](https://doi.org/10.1175/1520-0469(1989)046<3077:NSOCOD>2.0.CO;2).
- Emmons, L.K., Schwantes, R.H., Orlando, J.J., Tyndall, G., Kinnison, D., Lamarque, J.-F., Marsh, D., Mills, M.J., Tilmes, S., Bardeen, C., Buchholz, R.R., Conley, A., Gettelman, A., Garcia, R., Simpson, I., Blake, D.R., Meinardi, S., Pétron, G., 2020. The chemistry mechanism in the community earth system model version 2 (CESM2). *J. Adv. Model. Earth Syst.* 12 <https://doi.org/10.1029/2019MS001882> e2019MS001882.
- Fan, J., Leung, L.R., DeMott, P.J., Comstock, J.M., Singh, B., Rosenfeld, D., Tomlinson, J.M., White, A., Prather, K.A., Minnis, P., Ayers, J.K., Min, Q., 2014. Aerosol impacts on California winter clouds and precipitation during CalWater 2011: local pollution versus long-range transported dust. *Atmos. Chem. Phys.* 14, 81–101. <https://doi.org/10.5194/acp-14-81-2014>.
- Fan, J., Leung, L.R., Rosenfeld, D., DeMott, P.J., 2017. Effects of cloud condensation nuclei and ice nucleating particles on precipitation processes and supercooled liquid in mixed-phase orographic clouds. *Atmos. Chem. Phys.* 17, 1017–1035. <https://doi.org/10.5194/acp-17-1017-2017>.
- Fast, J.D., Gustafson, W.I., Easter, R.C., Zaveri, R.A., Barnard, J.C., Chapman, E.G., Grell, G.A., Peckham, S.E., 2006. Evolution of ozone, particulates, and aerosol direct radiative forcing in the vicinity of Houston using a fully coupled meteorology-chemistry-aerosol model. *J. Geophys. Res.-Atmos.* 111 <https://doi.org/10.1029/2005JD006721>.
- Grell, G.A., Dévényi, D., 2002. A generalized approach to parameterizing convection combining ensemble and data assimilation techniques. *Geophys. Res. Lett.* 29 <https://doi.org/10.1029/2002GL015311>, 38-1-38-4.
- Grell, G.A., Peckham, S.E., Schmitz, R., McKeen, S.A., Frost, G., Skamarock, W.C., Eder, B., 2005. Fully coupled “online” chemistry within the WRF model. *Atmos. Environ.* 39, 6957–6975. <https://doi.org/10.1016/j.atmosenv.2005.04.027>.

- Gunther, A., Karl, T., Harley, P., Wiedinmyer, C., Palmer, P.I., Geron, C., 2006. Estimates of global terrestrial isoprene emissions using MEGAN (Model of Emissions of Gases and Aerosols from Nature). *Atmos. Chem. Phys.* 6, 3181–3210. <https://doi.org/10.5194/acp-6-3181-2006>.
- Harpold, A., Brooks, P., Rajagopal, S., Heidebuchel, I., Jardine, A., Stielstra, C., 2012. Changes in snowpack accumulation and ablation in the intermountain west. *Water Resour. Res.* 48 <https://doi.org/10.1029/2012WR011949>.
- Henao, J.J., Mejía, J.F., Rendón, A.M., Salazar, J.F., 2020. Sub-kilometer dispersion simulation of a CO tracer for an inter-Andean urban valley. *Atmos. Pollut. Res.* 11, 928–945. <https://doi.org/10.1016/j.apr.2020.02.005>.
- Hornberger, G.M., Hess, D.J., Gilligan, J., 2015. Water conservation and hydrological transitions in cities in the United States. *Water Resour. Res.* 51 (6), 4635–4649. <https://doi.org/10.1002/2015WR016943>.
- Huang, G., Brook, R., Crippa, M., Janssens-Maenhout, G., Schieberle, C., Dore, C., Guizzardi, D., Muntean, M., Schaaf, E., Friedrich, R., 2017. Speciation of anthropogenic emissions of non-methane volatile organic compounds: a global gridded data set for 1970–2012. *Atmos. Chem. Phys.* 17, 7683–7701. <https://doi.org/10.5194/acp-17-7683-2017>.
- Huning, L.S., AghaKouchak, A., 2020. Global snow drought hot spots and characteristics. *PNAS* 117, 19753–19759. <https://doi.org/10.1073/pnas.1915921117>.
- Iacono, M.J., Delamere, J.S., Mlawer, E.J., Shephard, M.W., Clough, S.A., Collins, W.D., 2008. Radiative forcing by long-lived greenhouse gases: calculations with the AER radiative transfer models. *J. Geophys. Res.-Atmos.* 113 <https://doi.org/10.1029/2008JD009944>.
- Janjić, Z.I., 1994. The step-mountain eta coordinate model: further developments of the convection, viscous sublayer, and turbulence closure schemes. *Mon. Weather Rev.* 122, 927–945. [https://doi.org/10.1175/1520-0493\(1994\)122<0927:TSMCEM>2.0.CO;2](https://doi.org/10.1175/1520-0493(1994)122<0927:TSMCEM>2.0.CO;2).
- Janssens-Maenhout, G., Crippa, M., Guizzardi, D., Dentener, F., Muntean, M., Pouliot, G., Keating, T., Zhang, Q., Kurokawa, J., Wankmüller, R., Denier van der Gon, H., Kuenen, J.J.P., Klimont, Z., Frost, G., Darras, S., Koffi, B., Li, M., 2015. HTAP v2.2: a mosaic of regional and global emission grid maps for 2008 and 2010 to study hemispheric transport of air pollution. *Atmos. Chem. Phys.* 15, 11411–11432. <https://doi.org/10.5194/acp-15-11411-2015>.
- Jat, R., Gurjar, B.R., Lowe, D., 2021. Regional pollution loading in winter months over India using high resolution WRF-Chem simulation. *Atmos. Res.* 249, 105326 <https://doi.org/10.1016/j.atmosres.2020.105326>.
- Jha, V., Cotton, W.R., Carrió, G.G., Walko, R., 2021. Seasonal estimates of the impacts of aerosol and dust pollution on orographic precipitation in the Colorado River Basin. *Phys. Geogr.* 42 (1), 73–97. <https://doi.org/10.1080/02723646.2020.1792602>.
- Jirak, I.L., Cotton, W.R., 2006. Effect of air pollution on precipitation along the front range of the rocky mountains. *J. Appl. Meteorol. Climatol.* 45, 236–245. <https://doi.org/10.1175/JAM2328.1>.
- Khain, A.P., 2009. Notes on state-of-the-art investigations of aerosol effects on precipitation: a critical review. *Environ. Res. Lett.* 4, 015004 <https://doi.org/10.1088/1748-9326/4/1/015004>.
- Lohmann, U., 2017. Anthropogenic aerosol influences on mixed-phase clouds. *Curr. Clim. Change Rep.* 3, 32–44. <https://doi.org/10.1007/s40641-017-0059-9>.
- López-Romero, J.M., Montávez, J.P., Jerez, S., Lorente-Plazas, R., Palacios-Peña, L., Jiménez-Guerrero, P., 2021. Precipitation response to aerosol-radiation and aerosol-cloud interactions in regional climate simulations over Europe. *Atmos. Chem. Phys.* 21 (1), 415–430. <https://doi.org/10.5194/acp-21-415-2021>.
- Lynn, B., Khain, A., Rosenfeld, D., Woodley, W.L., 2007. Effects of aerosols on precipitation from orographic clouds. *J. Geophys. Res.-Atmos.* 112 <https://doi.org/10.1029/2006JD007537>.
- Mejia, J.F., Gillies, J.A., Etyemezian, V., Glick, R., 2019. A very-high resolution (20m) measurement-based dust emissions and dispersion modeling approach for the Oceano Dunes, California. *Atmos. Environ.* 218, 116977 <https://doi.org/10.1016/j.atmosenv.2019.116977>.
- Mesinger, F., DiMego, G., Kalnay, E., Mitchell, K., Shafran, P.C., Ebisuzaki, W., Jović, D., Woollen, J., Rogers, E., Berbery, E.H., Ek, M.B., Fan, Y., Grumbine, R., Higgins, W., Li, H., Lin, Y., Manikin, G., Parrish, D., Shi, W., 2006. North American regional reanalysis. *Bull. Am. Meteorol. Soc.* 87, 343–360. <https://doi.org/10.1175/BAMS-87-3-343>.
- Mlawer, E.J., Taubman, S.J., Brown, P.D., Iacono, M.J., Clough, S.A., 1997. Radiative transfer for inhomogeneous atmospheres: RRTM, a validated correlated-k model for the longwave. *J. Geophys. Res.-Atmos.* 102 (D14), 16663–16682. <https://doi.org/10.1029/97JD00237>.
- Mote, P.W., Li, S., Lettenmaier, D.P., Xiao, M., Engel, R., 2018. Dramatic declines in snowpack in the western US. *npj Clim. Atmos. Sci.* 1, 1–6. <https://doi.org/10.1038/s41612-018-0012-1>.
- Niu, G.-Y., Yang, Z.-L., Mitchell, K.E., Chen, F., Ek, M.B., Barlage, M., Kumar, A., Manning, K., Niyogi, D., Rosero, E., Tewari, M., Xia, Y., 2011. The community Noah land surface model with multiparameterization options (Noah-MP): 1. Model description and evaluation with local-scale measurements. *J. Geophys. Res.-Atmos.* 116 <https://doi.org/10.1029/2010JD015139>.
- Rosenfeld, D., Givati, A., 2006. Evidence of orographic precipitation suppression by air pollution-induced aerosols in the Western United States. *J. Appl. Meteorol. Climatol.* 45, 893–911. <https://doi.org/10.1175/JAM2380.1>.
- Rosenfeld, D., Dai, J., Yu, X., Yao, Z., Xu, X., Yang, X., Du, C., 2007. Inverse relations between amounts of air pollution and orographic precipitation. *Science* 315, 1396–1398. <https://doi.org/10.1126/science.1137949>.
- Rosenfeld, D., Woodley, W.L., Axisa, D., Freud, E., Hudson, J.G., Givati, A., 2008. Aircraft measurements of the impacts of pollution aerosols on clouds and precipitation over the Sierra Nevada. *J. Geophys. Res.-Atmos.* 113 <https://doi.org/10.1029/2007JD009544>.
- Saleeby, S.M., Cotton, W.R., Fuller, J.D., 2011. The cumulative impact of cloud droplet nucleating aerosols on orographic snowfall in Colorado. *J. Appl. Meteorol. Climatol.* 50, 604–625. <https://doi.org/10.1175/2010JAMC2594.1>.
- Saleeby, S.M., Cotton, W.R., Lowenthal, D., Messina, J., 2013. Aerosol impacts on the microphysical growth processes of orographic snowfall. *J. Appl. Meteorol. Climatol.* 52, 834–852. <https://doi.org/10.1175/JAMC-D-12-0193.1>.
- Sun, C., Liang, X.Z., 2020. Improving US extreme precipitation simulation: sensitivity to physics parameterizations. *Clim. Dyn.* 54, 4891–4918. <https://doi.org/10.1007/s00382-020-05267-6>.
- Svoma, B.M., Balling, R.C., 2009. An anthropogenic signal in Phoenix, Arizona winter precipitation. *Theor. Appl. Climatol.* 98, 315–321. <https://doi.org/10.1007/s00704-009-0121-1>.
- Thompson, G., Field, P.R., Rasmussen, R.M., Hall, W.D., 2008. Explicit forecasts of winter precipitation using an improved bulk microphysics scheme. Part II: implementation of a new snow parameterization. *Mon. Weather Rev.* 136 (12), 5095–5115. <https://doi.org/10.1175/2008MWR2387.1>.
- Toride, Kinya, Iseri, Yoshihiko, Duren, Angela, M., England, John, F., Kavvas, M. Leven, 2019. Evaluation of physical parameterizations for atmospheric river induced precipitation and application to long-term reconstruction based on three reanalysis datasets in Western Oregon. *Sci. Total Environ.* 658, 570–581. <https://doi.org/10.1016/j.scitotenv.2018.12.214>.
- USGCRP, 2018. Impacts, risks, and adaptation in the United States: fourth national climate assessment. In: Reidmiller, D.R., Avery, C.W., Easterling, D.R., Kunkel, K. E., Lewis, K.L.M., Maycock, T.K., Stewart, B.C. (Eds.), U.S. Global Change Research Program, Washington, DC, USA, Volume II: Report-in-Brief. <https://doi.org/10.7930/CA4.2018.RiB>, 186 pp.
- Wild, O., Zhu, X., Prather, M.J., 2000. Fast-J: accurate simulation of in- and below-cloud photolysis in tropospheric chemical models. *J. Atmos. Chem.* 37, 245–282. <https://doi.org/10.1023/A:1006415919030>.
- Zaveri, R.A., Peters, L.K., 1999. A new lumped structure photochemical mechanism for large-scale applications. *J. Geophys. Res.-Atmos.* 104, 30387–30415. <https://doi.org/10.1029/1999JD900876>.
- Zaveri, R.A., Easter, R.C., Fast, J.D., Peters, L.K., 2008. Model for simulating aerosol interactions and chemistry (MOSAIC). *J. Geophys. Res.-Atmos.* 113 <https://doi.org/10.1029/2007JD008782>.